Regular Article

Compressive creep behaviour of hot-pressed PbTe

C.C. Li [1], G.J. Snyder, D.C. Dunand *

Department of Materials Science & Engineering, Northwestern University, Evanston, IL 60208, USA

A B S T R A C T

Creep deformation is of concern in PbTe thermoelectric modules operating for years at high homologous temperatures while being subjected to internal or external stresses. The creep strain rates of hot-pressed PbTe are measured at 400 °C; a power-law is found, with a stress exponent $n = 1.7$ at low stresses (2–7 MPa) and $n = 4.4$ at high stresses (7–35 MPa). Creep rates measured at low stresses (4–6 MPa) between 350 and 500 °C provide a creep activation energy $Q = 181 \pm 18$ kJ/mol. The creep parameters and the good hot ductility of PbTe are compared to those for cast Bi_2Te_3 reported in the literature.

© 2017 Acta Materialia Inc. Published by Elsevier Ltd. All rights reserved.

1. Introduction

Thermoelectric materials, which convert heat into electrical energy, have been used for decades in radioisotope thermoelectric generator in space exploration [1–3] and more recently, to use waste heat from industrial processes [4] and internal combustion engines [5,6]. The main reliability concerns for thermoelectric modules are thermo-mechanical stresses from high thermal gradient [7,8], intermetallic growth at the interface with contacts [9–11], and sublimation of the thermoelectric material [12]. Design of devices must also take into account the temperature dependence of the Young's modulus with temperature, e.g., as measured between 20–300 °C for hot-extruded PbTe by Vasilevskiy et al. [13]. Furthermore, creep deformation is an issue for long-term dimensional stability, and can be expected to create sizeable deformation even at low stresses, given the very long times and high homologous temperatures at which modules are operated. Understanding the creep behaviour is also necessary to predict and optimize formability of thermoelectric materials at high temperature (e.g., by extrusion and forging) [14], and the kinetics of powder densification (e.g., during hot-isostatic pressing) [15].

Lead telluride (PbTe) is a high-efficiency thermoelectric material developed over the past decade [16] with optimized service temperature in the range 200–600 °C; PbTe displays a dimensionless thermoelectric figure of merit as high as $zT = \sim 2$, which could translate to an efficiency value of ~20% when incorporated into a device [17,18]. For a device hot-side temperature of 600 °C, PbTe is well within the creep regime [19], as the homologous temperature is $T/T_m = 0.73$, where $T_m = 1197$ K (924 °C) is the absolute melting temperature of PbTe. The material can be subjected to internal stresses (from thermal mismatch during isothermal or thermal cycling conditions) and external stresses (from clamping pressure or vibrations). In particular, the clamping pressure for thermoelectric modules embedded in power generation systems can be as high as 1.4 MPa [20].

To date, very few studies have addressed creep of thermoelectric materials. The compressive creep of cast, coarse-grained Bi_2Te_3 was measured between 400 and 500 °C for stresses between 2 and 16 MPa [21]. The parameters of the creep power-law (stress exponent and activation energies) were determined and a high creep anisotropy was found, implying that some crystallographic orientations are stronger than others. Creep activation energy was measured via internal friction between 27 and 377 °C on extruded bismuth telluride with nanometric grain size [22]. Furthermore, creep activation energy of $Bi_2Te_{28}Se_{02}$ single crystals was also characterized by microhardness between 30 and 100 °C [23]. The effect of the rate of plastic deformation in extrusion for n-$Bi_2(Te,Se)_3$ and p-$(Bi,Sb)_2Te_3$ at 400–500 °C has been studied [24]. Nb-doped $(GeTe)_x(Mn_{0.6}Sn_{0.4}Te)_{1-x}$ was found to be quite creep resistant, showing a strain of <0.4% after 100 h under a stress of 2.6 MPa at 600 °C [25]. Also studied were n- and p-PbTe specimens which showed a transition from logarithmic to exponential creep at $T/T_m = 0.5$ and 0.4, respectively [26].

The present paper reports on the compressive creep behaviour of hot-pressed PbTe, during creep experiments performed for various stresses at 350–500 °C for times up to 170 h. The creep power-law parameters are determined and discussed in the light of likely creep deformation mechanisms. Compressive ductility is also assessed.

---

* Corresponding author.
  E-mail address: dunand@northwestern.edu (D.C. Dunand).
[1] Currently at Industrial Technology Research Institute of Taiwan, R.O.C.

2. Experimental procedures

Equiatomic PbTe ingots were prepared by melting powders of Pb and Te (both 99.999%, from Alfa Aesar) in an evacuated quartz tube at 1000 °C for 6 h, followed by solidification and annealing at 700 °C for 48 h to ensure homogeneity. The PbTe ingots were ball-milled dry in a SPEX mill into micron-scale powders in an Ar atmosphere for 1 h, using 316 stainless steel. Powder X-ray diffraction patterns showed that the PbTe powders were single phase with the NaCl crystal structure. A quantity of 10 g of PbTe powders was poured into a graphite die and then subjected to spark plasma sintering (using a SPS-511S, SPS SYNTEX INC.) and isothermally sintered for 15 min under vacuum at pressure and temperature of 60 MPa and 550 °C, respectively. The pressure was then released and the samples were allowed to cool to 60 °C in ~1 h. For grain size determination, the samples were mounted in epoxy resin, ground using a series of SiC papers from 400 to 2000 grit, and then polished with Al_2O_3 powder suspensions (1 and 0.05 μm). The metallographic observations (secondary ion images) were obtained using a Focused Ion Beam Microscope (FEI helios 600i). The thermoelectric properties of these hot-pressed PbTe were characterized in our previous study [27].

Creep specimens were cut from the pressed ingot with a diamond saw into 4x4x10 mm^3 tetragonal prisms.Constant-load creep tests, with compressive stresses in the range of 2.2–35 MPa, were performed in air at 350, 400, 450 and 500 °C, corresponding to a range of homologous temperatures of 0.52–0.65.A nickel-base superalloy creep cage translated tensile loads in the pull-rods to compressive stresses on the specimen. Frictional effects on the end-loaded specimens were minimized using alumina platens coated with boron nitride. Specimen temperature was measured in the three-zone furnace with a temperature stability of ± 1 °C after a 1 h soak at the test temperature. Specimen strain was calculated from displacements of cage platens measured with a resolution of 2.5 μm in the cold zone via an extensometer outfitted with a linear variable differential transducer (LVDT). Two types of measurements were carried out.First, isothermal creep experiments were performed at 400 °C on four specimens (labelled A-D): starting from a low stress, a steady-state strain rate is achieved and measured, and then the procedure is repeated at a higher stress, resulting in 2–5 data points suitable for determining the stress exponent from a single specimen. Second, constant load experiments were carried out on two specimens (E, F) at 4.5 and 5.6 MPa respectively. Once reaching the designated temperature and soaked for 1 h for stability of ± 1 °C, the load is applied and the steady-state strain rate, once achieved, is measured; the procedure is repeated at two higher temperatures, resulting in three data points used to determine the activation energy.

3. Results and discussion

Fig. 1 (a) and (b) show secondary ion images of the PbTe specimens in the as-pressed and aged (336 h at 400 °C) conditions, respectively. The grain size distribution appears bimodal, with about half the cross-section occupied with fine grains, ~10–25 μm in size, and the other half with larger grains, ~50–150 μm in size. There is no evidence of grain growth after thermal treatment, so that grain size can be assumed to be constant during the creep experiments, whose longest duration was 170 h at 400 °C.

Fig. 2(a) and (b) shows the creep curves at 400 °C for specimens A-D. A primary creep period, where the strain rate decreases continuously with time, always precedes steady-state creep (secondary creep). The strain accumulated during primary creep is substantial (~0.5–1%) and stretches over long times (up to 73 h for sample B tested at 3.3 MPa); this regime is associated with the establishment of a steady-state dislocation structures within grains and at grain boundaries, and the balancing between strain hardening and softening. The minimum strain rate associated with the secondary creep regime is plotted as a function of applied stress in Fig. 2 (b) for the four tests performed at 400 °C. The
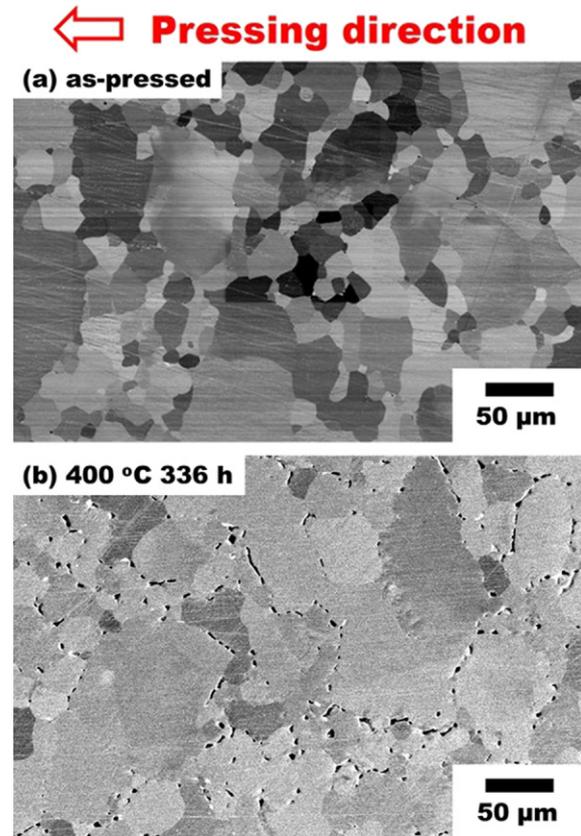

Fig. 1. Secondary ion micrograph of polished cross-section of hot-pressed PbTe (a) before annealing (unetched) and (b) after annealing at 400 °C for 336 h (pores created by 68 wt% HNO_3 etchant).

data can be described by a power-law creep eq.[19]:

$$\dot{\varepsilon} = A\sigma^n \exp\left(-\frac{Q}{R_g T}\right) \tag{1}$$

where $\dot{\varepsilon}$ is the minimum, secondary strain rate, A is a constant, σ is the applied stress, n is the stress exponent, Q is the activation energy for creep, R_g is the gas constant, and T is the absolute temperature. Fig. 2 (c) shows stress exponents $n = 1.7$–2.2 at low stresses (samples A-C) and $n = 4.4$ at higher stresses (sample D). The higher stress exponent ($n = 4.4$) is in the same range as those measured for ionic compounds ($n = 3.3$ for MgO, 3.6 for NaCl and 4.2 for FeO) [19]. More generally, in all crystalline materials, diffusional creep at low stresses is characterized by $n = 1$–2, and dislocation creep at higher stress is associated with $n = 3$–8 [19].

As shown in Fig. 2 (d), where the 400 °C creep data from Fig. 2 (a) for different specimens are aggregated, there is a clear transition from diffusional creep ($n = 1.6$) to dislocation creep ($n = 4.9$) at 7.3 MPa. As the transition occur rather sharply, the bimodal grain distribution does not appear to stretch the stress range where both mechanisms are contributing to the strain rate with similar magnitude in the two regimes. For comparison, creep data are also plotted for cast Bi_2Te_3 with large, elongated grains (~2–4 mm in length and ~0.1–0.3 mm in width) with basket-weave structure [21]. At a given stress, the strain rates are lower by a factor ~ 3–25, despite the lower melting point of Bi_2Te_3 as compared to PbTe, while the stress exponents are 4.2–6.2; the considerable sample-to-sample variation for Bi_2Te_3 was assigned to creep anisotropy in the large-grain samples [21]. The different crystal structure, as well as the different grain size, shape and solidification texture as compared to PbTe may contribute to the higher creep resistance of Bi_2Te_3.
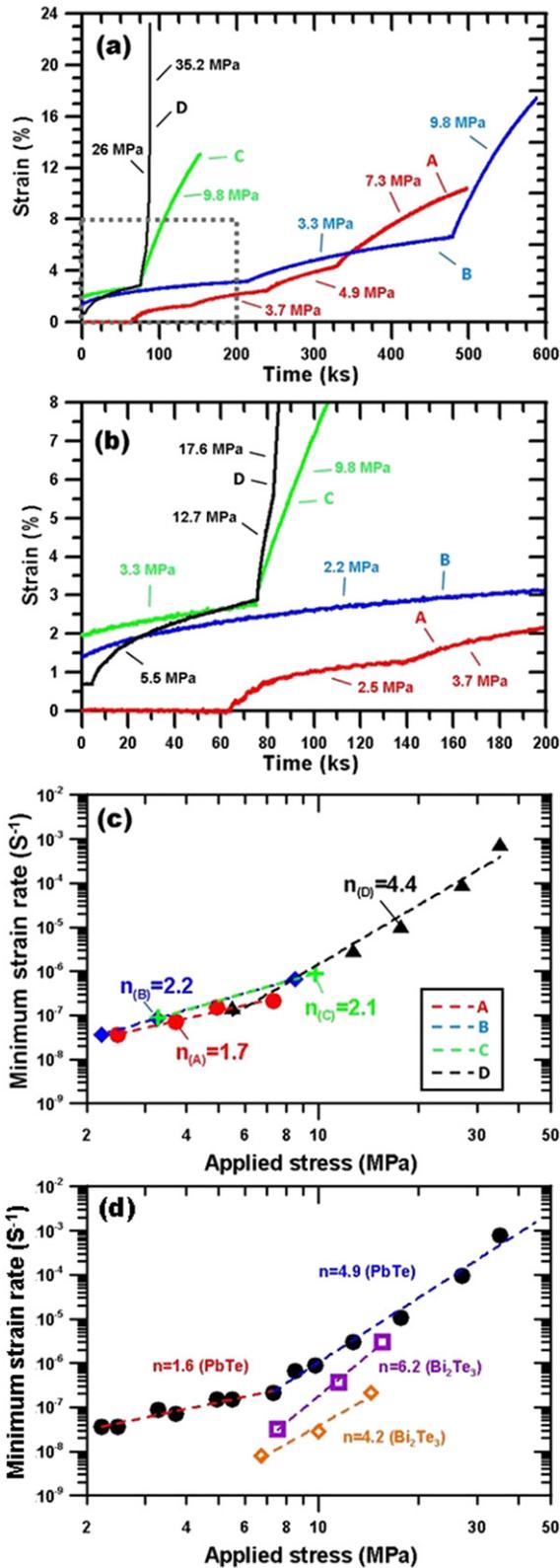
Fig. 2. Creep curves of PbTe at 400 °C for samples A-D subjected to increasing stresses. (a) Full experimental time span (b) Shorter time view of the grey region of (a). (c) Double logarithmic plot of minimum creep rate vs. applied stress for PbTe at 400 °C, with best-fit lines showing average stress exponent. (d) Double logarithmic plot of minimum creep rate vs. applied stress for creep of PbTe, showing average best-fit stress exponent at low and high stresses. Creep data for cast, coarse-grained Bi_2Te_3 at 400 °C are shown for comparison [21].

PbTe creep data at constant stress, collected on samples E and F at various temperatures, are plotted in Arrhenius form in Fig. 3, from which the activation energy for steady-state creep can be calculated based on Eq. (1): $Q = R_g[d(\ln\dot\varepsilon)/d(1/T)]$ [28]. For an applied stress of 4.5 MPa (sample E) and 5.6 MPa (sample F), best-fit procedures provide activation energies of 199 and 163 kJ/mol, respectively, with an average $Q = 181 \pm 18$ kJ/mol between 350 and 500 °C ($T/T_m = 0.52$–0.65). By comparison, the activation energy for cast Bi_2Te_3 is $Q = 145$ kJ/mol (with estimated error of ~25 kJ/mol) for an applied stress of 8.5 MPa between 400 and 500 °C ($T/T_m = 0.78$–0.90) [21]. Two data points for Bi_2Te_3 are plotted in Fig. 3 at 450 and 500 °C for a comparable stress of 5 MPa, again showing the higher creep resistance of Bi_2Te_3 as compared to PbTe. Direct comparison between the two materials is not possible, since the activation energy for PbTe corresponds to the low-stress regions associated with diffusional creep, while that for Bi_2Te_3 is in the high-stress dislocation creep regime. Furthermore, the homologous temperatures ranges do not overlap.

Fig. 4 shows the PbTe specimens A-D after creep at 400 °C, demonstrating a high level of plasticity, unlike Bi_2Te_3 which failed catastrophically in compression at 400 and 450 °C and showed a mixture of cracking and plastic deformation at 500 °C [21]. Samples E and F are not shown but deformed in a similar manner, with total strains of 21 and 12%, respectively. The barreling in specimen D (Fig. 4) is indicative of friction against the platens, and is expected given the high total strain of 23%. The good high-temperature compressive ductility observed here is consistent with experiments at ambient temperature on powder-metallurgy-prepared PbTe (undoped and doped), where strains at maximal compression stress were reported in the range 6–25% [29]. It can be concluded that powder-metallurgy PbTe is more ductile than cast Bi_2Te_3 up to 500 °C, which is relevant not only to resistance to mechanical fracture or fatigue during operation of thermoelectric devices, but also to formability (by extrusion or forging) and kinetics of powder densification (by hot isostatic pressing) during device processing.

4. Conclusions

The present study investigated the compressive creep behaviour of hot-pressed PbTe with bimodal grain size, which is relevant to the long-term reliability of thermoelectric power generation system subjected to internal or external stresses at high homologous temperatures. For uniaxial compressive stresses between 2.2 and 35 MPa at 400 °C, the stress dependence of the minimum strain rate can be characterized by a power-law with stress exponents $n = 1.6$ (below 7.3 MPa) and $n = 4.9$ (above 7.3 MPa), which are interpreted to correspond to the diffusional
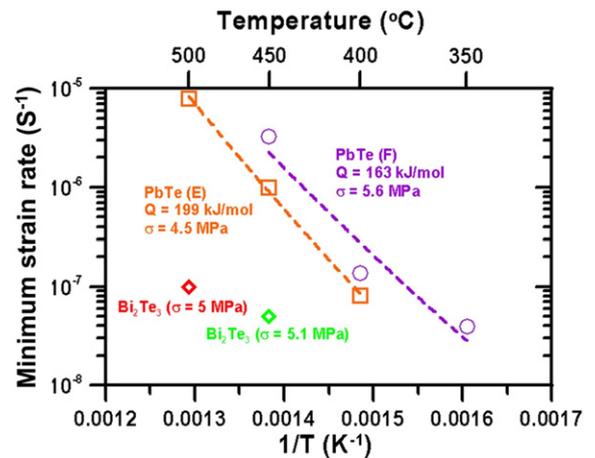

Fig. 3. Arrhenius plot of minimum creep rate vs. reciprocal temperature for PbTe, sample E (4.5 MPa) and F (5.6 MPa), showing best-fit creep activation energies. Data for coarse-grained Bi_2Te_3 at 400 °C are shown for comparison [21].
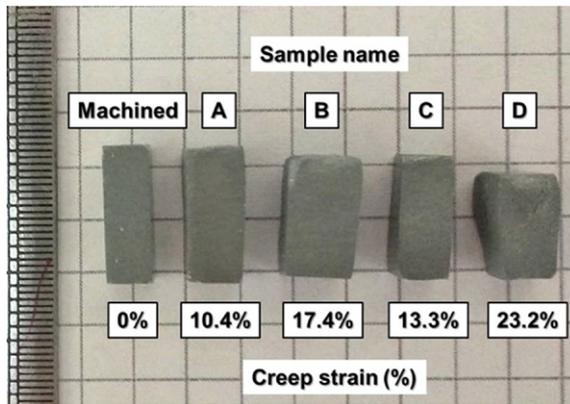
Fig. 4. Photographs of PbTe specimen before deformation and specimens A–D after creep deformation at 400 °C.

and dislocation creep regimes, respectively. An activation energy of 181 ± 18 kJ/mol is measured between 350 °C and 500 °C in the low-stress regime. In compression at 400 °C, PbTe shows a high level of plasticity without fracture, unlike cast coarse-grained Bi_2Te_3 which is brittle at 400 and 450 °C.

Acknowledgement

References

[1] R.W. Fritts, Thermoelectric Materials and Devices, Reinhold Pub. Corp., New York, 1960.
[2] R.R. Heikes, R.C. Miller, R.W. Ure, Thermoelectricity: Science and Engineering, Interscience Publishers, New York, 1961.
[3] Y.I. Ravich, B.A. Efimova, I.A. Smirnov, Semiconducting Lead Chalcogenides, Plenum Press, New York, 1970.
[4] T. Kuroki, K. Kabeya, K. Makino, T. Kajihara, H. Kaibe, H. Hachiuma, H. Matsuno, A. Fujibayashi, J. Electron. Mater. 43 (2014) 2405–2410.
[5] E.F. Thacher, B.T. Helenbrook, M.A. Karri, C.J. Richter, Part D: Journal of Automobile Engineering 221 (2007) 95–107.
[6] X. Liu, C.G. Yu, S. Chen, Y.P. Wang, C.Q. Su, J. Electron. Mater. 43 (2014) 2218–2223.
[7] Th. Clin, S. Turenne, D. Vasilevskiy, R.A. Masut, J. Electron. Mater. 38 (2009) 994.
[8] W. Liu, H.S. Kim, Q. J., Z. Ren, Scr. Mater. 111 (2016) (3).
[9] H. Xia, F. Drymiotis, C.L. Chen, A. Wu, G.J. Snyder, J. Mater. Sci. 49 (2014) 1716.
[10] C.C. Li, F. Drymiotis, L.L. Liao, H.T. Hung, J.H. Ke, C.K. Liu, C.R. Kao, G.J. Snyder, J. Mater. Chem. C 3 (2015) 10590.
[11] T.H. Chuang, W.T. Yeh, C.H. Chuang, J.D. Hwang, J. Alloys Compd. 46 (2014) 613.
[12] H.E. Bates, Martin Weinstein, Adv. Energy Convers. 6 (1966) (177).
[13] D. Vasilevskiy, R.A. Masut, S. Turennem, J. Electron. Mater. 41 (2012) 1057–1061.
[14] G.E. Dieter, D.J. Bacon, Mechanical Metallurgy, McGraw-Hill, London, 1988.
[15] M. Ito, K. Kawahara, Mater. Trans. 56 (2015) 2023.
[16] G.J. Snyder, E.S. Toberer, Nat. Mater. 7 (2008) 105.
[17] K. Biswas, J. He, I.D. Blum, C.I. Wu, T.P. Hogan, D.N. Seidman, V.P. David, M.G. Kanatzidis, Nature 489 (2012) (414).
[18] Y. Pei, H. Wang, G.J. Snyder, Adv. Mater. 24 (2012) 6125.
[19] J.J. Frost, M.F. Ashby, Deformation-Mechanism Maps: the Plasticity and Creep of Metals and Ceramics, Pergamon, New York, 1982.
[20] G.J. Snyder, A. Borshchevsky, A. Zoltan, T. Caillat, J.-P. Fleurial, B. Nesmith, J. Mondt, T. McBirney, D. Allen, J.C. Bass, S. Ghamaty, N. Elsner, L. Anatychuk, Proceedings of 21th International Conference on Thermoelectrics, IEEE, Long Beach, California, USA, 2002 463.
[21] Z.P. Guan, D.C. Dunand, Mater. Sci. Eng. A 565 (2013) 321.
[22] D. Vasilevskiy, O. Bourbia, S. Gosselin, S. Turenne, R.A. Masut, J. Electron. Mater. 40 (2011) 1046–1051.
[23] C.F. Desai, P.H. Soni, S.R. Bhavsar, Bull. Mater. Sci. 22 (1999) 21–23.
[24] O.B. Sokolov, S. Ya, Skipidarov, N.I. Duvankov, J. Thermoelectric 1 (2004) 48–54.
[25] L. Zhang, W. Wang, B. Ren, Y. Yan, J. Electron. Mater. 40 (2011) 1057.
[26] L.A. Evmen'ev, V.A. Mazur, Eh.S. Tipikina, Neorganicheskie Materialy 11 (1975) 1981.
[27] C.C. Li, F. Drymiotis, L.L. Liao, M.J. Dai, C.K. Liu, C.L. Chen, Y.Y. Chen, C.R. Kao, G.J. Snyder, Energy Convers. Manag. 98 (2015) 134–137.
[28] M.E. Kassner, M.T. Perez-Prado, Prog. Mater. Sci. 45 (2000) 1.
[29] Y. Gelbstein, G. Gotesman, Y. Lishzinker, Z. Dashevsky, M.P. Dariel, Scr. Mater. 4 (2008) 251.